ERDC/TN DOER-R27
August 2018

Improving Spatial Monitoring of Dredging Operations: A Small Unmanned Aerial System Application to Map Turbidity

by Justin L. Wilkens, Burton C. Suedel, Austin V. Davis, and Jeffrey M. Corbino

PURPOSE: There is interest in developing small unmanned aerial system (sUAS <25 kg) applications to improve the effectiveness and efficiency for monitoring turbidity associated with dredging operations. This technical note describes a method for using sUAS technology to monitor turbidity.

INTRODUCTION: Dredging operations resuspend sediment, creating a plume in the water column. Other turbidity plumes associated with the discharge of dredged material may be a concern in waters adjacent to placement sites. Assessment of the plume's spatial extent is vital when complying with regulations at the dredging and placement sites (Reine et al. 1998; Suedel et al. 2008). Plume characterization focuses on the measurement of turbidity (i.e., nephelometric turbidity units) (NTU) and total suspended solids (TSS in mg/L) (Clarke and Wilber 2008; Pruitt 2003). Such data, along with knowledge of ambient conditions, determines the impact of dredge or placement area plumes, and can result in modification to dredging and disposal operations, when needed (Puckette 1998; Clarke and Wilber 2008). To minimize potential harm, dredging operations require monitoring, typically from manned boats that have spatial and temporal limitations. Additionally, regulations sometimes prohibit the use of motorized boats near ecologically sensitive areas. In some instances, conventional methods (e.g., direct measurement) limit the quantification of a plume's concentration, frequency, and duration, thereby inadequately evaluating effective dredging management practices.

To improve spatial monitoring, images of turbidity can be obtained from satellites (Kutser et al. 2007) or manned flights (Roberts et al. 1995) and correlated to in situ water sampling. However, depending on the needs of the application, satellite remote sensing technologies can be limited. The coarse spatial and temporal granularities of satellite imagery may be impractical to use for determining the short-term impacts, such as a dredge plume on a specific area. Satellites do not revisit areas often (i.e., one pass per day) and cloud obscuration can make imagery unusable. Manned aircraft provide higher spatial and temporal resolution imagery, but expensive image acquisition and operating costs make manned flights impractical. Additionally, cloud obscuration is still an issue. Recent developments in sUAS technologies provide an inexpensive alternative for acquiring imagery (Watts et al. 2010). A sUAS is a lightweight unmanned aircraft capable of manual, assisted, or autonomous flight. The sUASs fly at lower elevations and thus are capable of collecting imagery with high spatial and temporal resolution (e.g., 5 cm/pixel, 10 minute revisit time). Therefore, sUAS can compete with traditional mapping solutions (Küng et al. 2011).

A method used to integrate sUAS aerial imagery with in situ water samples is presented in this technical note. Georeferenced images of turbidity were integrated with geographical information systems (GIS) to map the test area with a relative turbidity classification. Finally, the workflow for obtaining remote sensing data is discussed.

METHODS: The field test occurred at a distributary channel located near the mouth of the Atchafalaya River (29°26'58.52"N, 91°20'15.65"W) in southern Louisiana (Figure 1). Turbidity near the water surface was relatively low, homogenous (≈15-55 NTU) and originated from ambient sources. The sUAS was deployed from a clearing near the distributary channel.

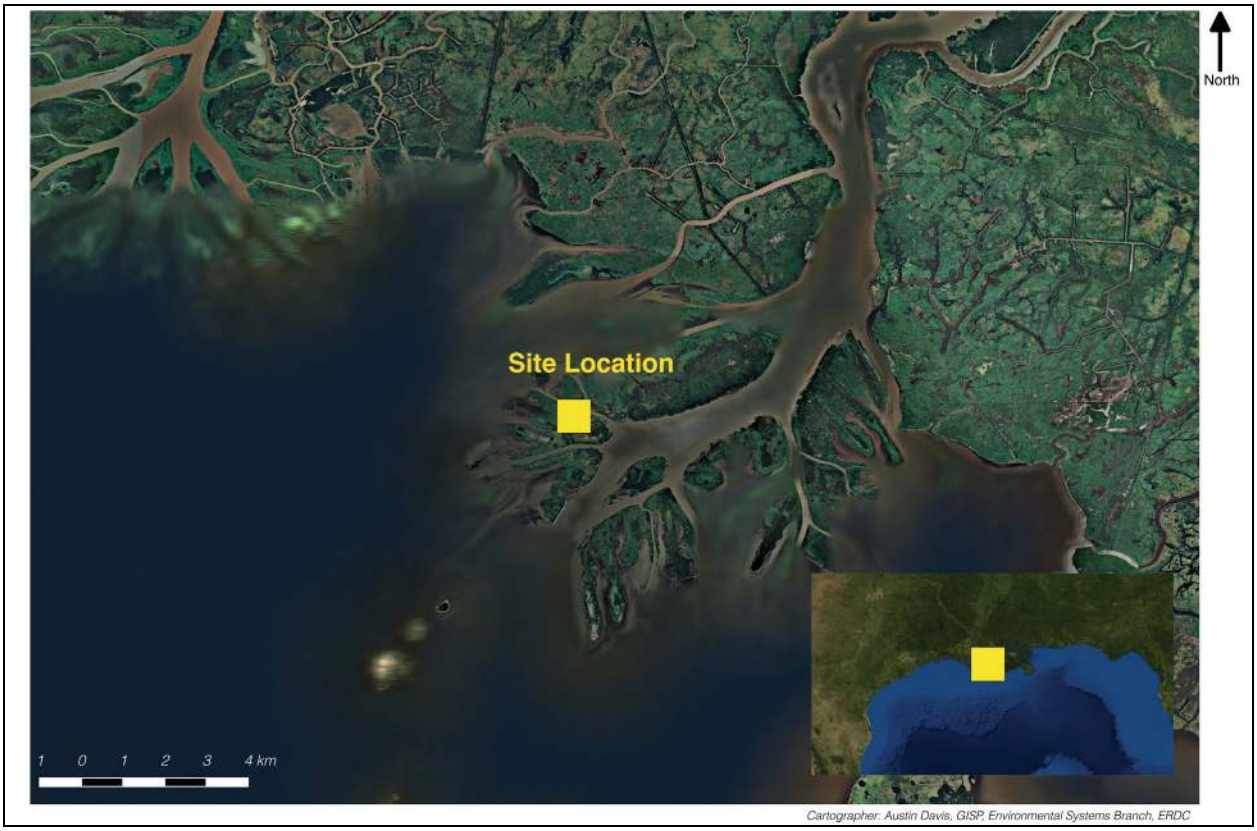

Figure 1. The study site and location of the distributary channel near the mouth of the Atchafalaya River, LA.

An autonomous, line-of-site flight was conducted using an eBeeRTK (senseFly, Switzerland, sensefly.com) (Figure 2), which is a fixed-wing ultra-light sUAS equipped with a digital camera (Canon S110 Near-infrared [NIR] 12 megapixel, Canon, Tokyo, Japan). This lithium-polymer battery powered drone acquires geospatially tagged images over programmed flight paths. The eBee has a foam fuselage and includes all electronics, built-in autopilot, and detachable wings. The sUAS's wingspan is 96 cm and it weighed 0.73 kg (including camera and battery). The eBee is equipped with a rear facing electric motor. The eBee can fly for approximately 40 minutes at cruising speeds of 11–25 m/s and can withstand winds up to 45 kmh. The eBee is hand launched, thus there is no need for a special catapult device or runway. To land, the sUAS glides downward and then is manually skid-landed.

Figure 2. Fixed-wing senseFly eBeeRTK used to acquire aerial images.

The eBee was equipped with a Global Navigation Satellite System (GNSS); L1/L2, Global Positioning System (GPS) and Global Navigation Satellite System (GLONASS). Absolute horizontal and vertical accuracy without ground control points (GCPs) was 3 cm and 5 cm, respectively, as reported by Roze et al. (2014). GCPs are features on the Earth's surface of known locations and can be used to geo-reference image data to increase accuracy. Achieving high accuracy without GCPs was an important, time saving feature when competing with the simplicity of in situ turbidity measurements. Additionally, the distributary channel was in a remote area making GCPs impractical. The eBee payload was a Canon S110 NIR sensor (weight ≈ 180 g; size 98.8 x 59.0 x 26.9 mm). This sensor acquired 12.1 megapixel images in the visible (green 550 nm; red 625 nm) and NIR (850 nm) spectrum. SenseFly modified the camera so the autopilot controlled when the camera acquired images based on user input made during flight planning. To prevent blurred images caused by vibrations, the eBee autopilot briefly stopped the engine, stabilized in a level attitude then triggered the camera. The eBee then resumed the programmed flight path and quickly corrected course. Other relevant camera parameters included an approximate nadir ground resolution at 100 m, of 3.5 cm/pixel, sensor size of 7.44 x 5.88 mm, pixel pitch of 1.86 μm, JPEG and/or RAW image format and shutter speed of 1/2000 sec.

The eBee flight planning software (eMotion) was used to plan and control the flight on a laptop (Windows 7). The flight was programmed to systematically cover the test area with 75% lateral and longitudinal overlap at an altitude of 180 m. Images were directly georeferenced, whereby, the onboard GNSS and inertial measuring unit determined the position and orientation of the camera. After the flight, Pix4Dmapper (Pix4D, Switzerland) photogrammetry software was used to process the images to create an orthomosaic image of the test area. The automated process used an algorithm, known as scale-invariant feature transform, to match points between the images (Lowe 2004). The geotag provided by the sUAS autopilot determined image position and orientation. This post image processing was robust in that it provided a "one click" solution.

Within one-hour, post-flight in situ water samples (500 ml) were collected to correlate with sUAS images. Due to low water currents, wind (≈0.5 m/s), and relatively homogenous turbidity conditions, the samples were considered representative of the acquisition time of the aerial images. Within the sUAS image acquisition area, collection of water samples occurred at 14 sites.

Sampling locations were determined in the field and were considered representative for monitoring the study area (<1 km^2) mapped by aerial images (Figure 3).

Each sampling location was marked using a GPS (Trimble SPS 5800, Sunnyvale, CA, USA). Plastic bottles (250 ml) rinsed with water from each location were refilled with water collected near the surface (i.e., top 10 cm). The samples were used for laboratory analysis of turbidity and TSS. To minimize microbiological decomposition of solids prior to analysis, samples were kept at 4°C. The post-sample laboratory process utilized a turbidimeter (Hach 2100Q, Loveland, CO, USA) to measure turbidity of the hand-collected samples. Values used represented the mean three turbidity measurements taken from each sample (Table 1). For TSS, the water sample was hand mixed using a wide-mouthed pipette, a 100 ml sample was collected. The samples were transferred to a filter apparatus and the pipette was rinsed with deionized water to ensure all sediment was transferred. A vacuum was applied to the apparatus and all water was drawn through the pre-weighed filter (0.45 µm, Millipore, Billerica, MA, USA). Then, the filter funnel and filter were rinsed with deionized water and vacuum filtered again to remove all water. The filter and contents were dried at 105°C overnight then reweighed to the nearest 0.0001 g using an analytical balance (MS104TS, Mettler Toledo, Columbus, OH, USA).

Figure 3. Water sampling sites in distributary channel near the mouth of the Atchafalaya River, LA, on 22 June 2016.

Table 1. Results of water quality measurements taken of samples collected near the water surface (top 15 cm) on 22 June 2016.

	Laboratory			Field Location and Time		
Sample	Turbidity (NTU)	TSS (mg/L)		Latitude	Longitude	Time
1	15.7	19		29.448287	-91.33823	11:49:32 AM
2	16.1	18		29.448753	-91.338029	11:53:02 AM
3	24.3	26		29.449329	-91.337747	11:54:12 AM
4	49.8	53		29.450196	-91.33914	11:57:02 AM
5	49.1	54		29.450323	-91.339605	11:58:12 AM
6	48.1	50		29.45072	-91.340248	12:00:07 PM
7	47	52		29.451009	-91.340563	12:03:27 PM
8	47.4	58		29.450388	-91.339059	12:06:07 PM
9	49.9	60		29.449646	-91.33821	12:08:42 PM
10	54.3	76		29.449307	-91.336642	12:11:42 PM
11	51.8	66		29.449455	-91.335401	12:14:27 PM
12	47.9	59		29.449724	-91.334275	12:16:57 PM
13	48.8	58		29.448976	-91.333709	12:19:37 PM
14	50.5	58		29.448872	-91.332715	12:21:42 PM

The orthomosaic, overlaid with water sample locations, was used to create a map and a color bar to display the relative concentration estimates of turbidity of the pixels representing the channel. The Semi-Automatic Classification Plugin for Quantum GIS created a relative turbidity classification by manually selecting and classifying training areas with different spectral signatures using a manual delineation (Congedo 2016). Ideally, creation of several training areas is desirable when considering the spectral variability that is possible for different turbidity levels. Without a color reference to help spectrally calibrate an image, precise and accurate measures of turbidity were not possible. However, observations of the data suggest that regions of lower spectral intensity in the waterway represented lower NTU values. This pattern was evident in the water samples collected at various locations. Segmenting the intensity values into two categories produced a map, such that areas classified within the lower intensity category were estimated to represent areas of turbidity below 25 NTU.

RESULTS AND DISCUSSION: One line-of-site flight (≈25 min) conducted on 22 June 2016, acquired images of the distributary channel. Weather conditions were: wind speed of 0.5 m/s from the south-southeast with a maximum wind speed of 5 mph; visibility 10 miles; and scattered clouds (above flying area). The sUAS covered an area of approximately 60 hectares at a height of 180 m with a ground resolution of 5.2 cm/pixel. Acquired images produced a 3D point cloud and mesh, a digital surface map, orthomosaic, and classification (Figure 4). A map created by classifying the orthomosaic image visually estimated water quality parameters based on a color scale (Figure 5).

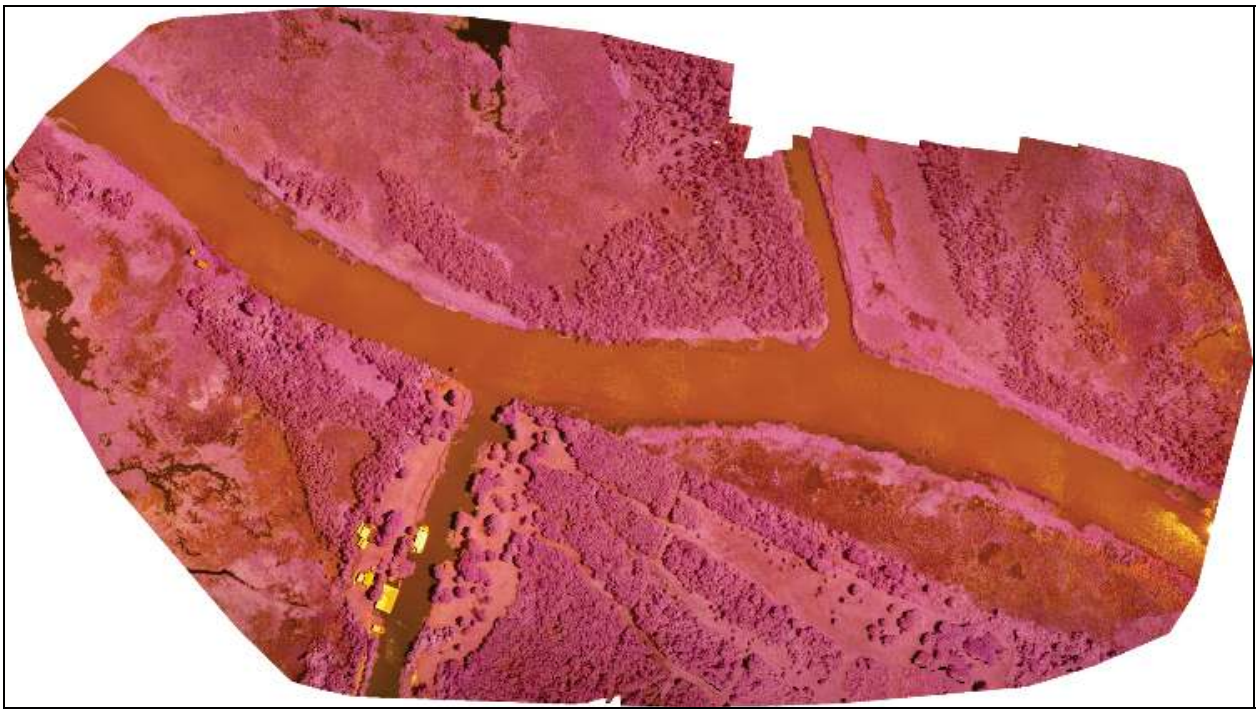

Figure 4. Georeferenced orthomosaic created with near infrared aerial images of the distributary channel near the mouth of the Atchafalaya River, LA, on 22 June 2016.

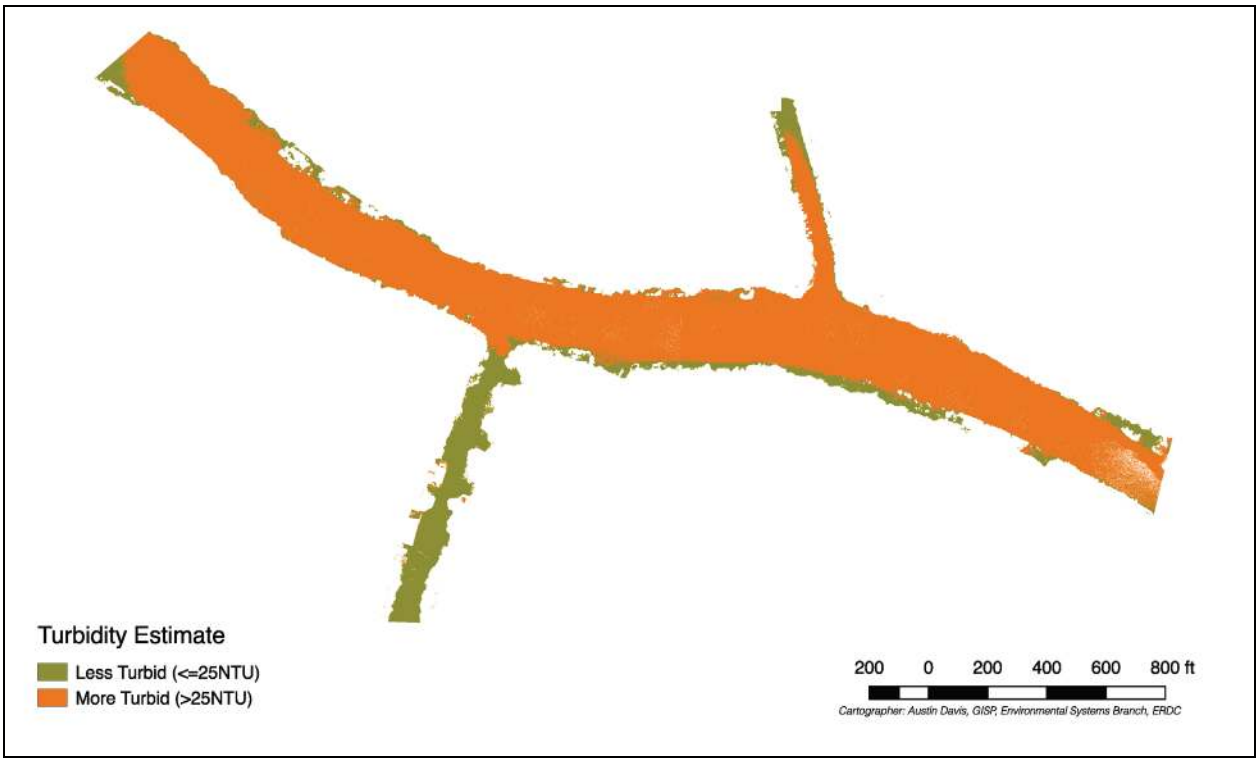

Figure 5. Map of estimated turbidity levels and total suspended solid concentrations correlated with in situ water samples of a distributary channel near the mouth of the Atchafalaya River, LA, on 22 June 2016.

Combining the map overlay with in situ water samples allowed for evaluation of turbidity and TSS concentrations over a much broader area. The high ground resolution (5.2 cm/pixel) offered sufficient contrast for areas with relatively homogenous turbidity (i.e., < 25 or > 25 NTU). Figure 6 displays the workflow for developing the sUAS remote sensing application.

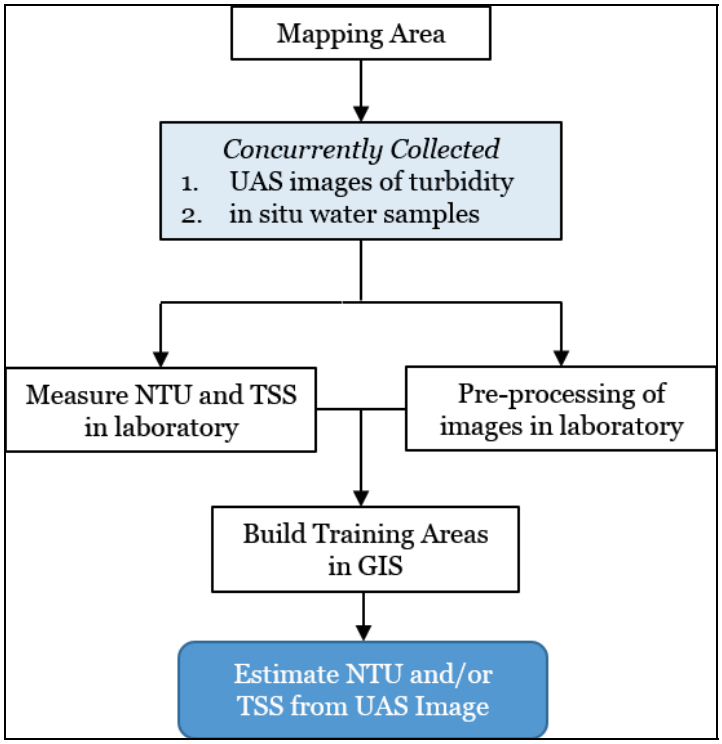

Figure 6. Flowchart of the steps used to generate the relationships between turbidity and NIR using sUAS technology.

When visually estimating turbidity with sUAS images, it is important to correlate turbidity levels with spectral signatures to predict related water quality parameters. If the turbidity-spectral signature relationship is weak or spectrally uncalibrated, it may only be useful for establishing general trends and will be unable to provide an accurate visual estimate. To develop an accurate characterization and classification system for turbidity measurement using sUAS imagery, placement of sub-surface spectral calibration panels within a subset of the images should help perform spectral calibration. Further, the calibration panel should be associated with a turbidity sensor to help predict turbidity across the geographic space. However, even when successfully calibrated, Lui et al. (2003) found the models are site specific and require daily calibration. Therefore, daily flights and in situ sampling are likely required to build accurate regression models. Automation of these processes with, for example, turbidity data loggers could help decrease effort. Currently, the discrimination of turbidity levels using sUAS images does not provide real time turbidity monitoring data collected in near real time in the field, from a manned vessel, and from data loggers.

Although there may be limitations to real time data retrieval, sUASs still have the potential to increase the spatial assessment of sediment plumes in comparison to conventional manned vessel

methods while providing the necessary accuracy (Vogt and Vogt 2016). In terms of a dredging operation, the movement of plumes and dissipation over space and time is important for predicting potential impacts associated with dredging. There are challenges in characterizing dredge plumes because of their variable nature. The nature and extent of a dredge plume is mostly the result of the dredge type, hydrodynamics, and sediment characteristics. A plume may exhibit systematic patterns of distribution influenced by local environmental conditions from the onset of the plume to resettling; but such conditions may only persist for short periods before changing, especially near the dredge. Therefore, it may be challenging, for instance, to collect water samples that are representative of the aerial images. However, even if calibration fails to provide accurate measurement, georeferenced images can still provide relative estimates as evidence of the plumes' spatial scale and proximity to sensitive habitats that manned vessels could not otherwise easily obtain. This information could support better-informed regulations and dredging strategies, especially when applying additional steps to calibrate the spectral signature of images with in situ water samples.

Depending on the dredge method, the sediment plume may be more concentrated near the bottom of the water column; thus, a sUAS image sensor's ability to penetrate the water column and the clarity of the overlying water may limit its application to shallow water. Alternatively, an unmanned surface vehicle (USV) could monitor turbidity. A USV is a small surface vessel capable of manual or autonomous operation. USVs are capable of bathymetry mapping as well as mapping aquatic habitats (Legleiter et al. 2014; Tedesco and Steiner 2011). They are ideal for shallow water, tidal, and other hard-to-access areas. A USV can be equipped with a pump to collect water samples for turbidity measurement. Side scan sonars, acoustic Doppler current profilers, and other sensors attached to the USV can analyze a plume below the water surface. USV technologies may be another flexible option to create dredging monitoring applications and would provide complementary information with sUAS images.

CONCLUSION: sUAS technologies offer a more viable and flexible alternative to conventional platforms such as satellites and manned aircraft. This study demonstrated relatively uniform turbidity levels can be differentiated using high-resolution ground images on the centimeter scale relatively calibrated to in situ water samples. Images were of turbidity near the water surface thus this application would be most appropriate for assessing turbidity near the surface or in shallow water habitats (e.g., sea grass and coral reefs). Integrating sUAS technology with dredging operations will improve spatial monitoring of sediment plumes occurring near the water surface or in shallow water areas and will produce evidence-based information about the plume's scale to enable better-informed regulations and dredging strategies.

POINTS OF CONTACT: For additional information, contact Justin Wilkens (601-634-2421), *Justin.L.Wilkens@usace.army.mil*) or Dr. Burton Suedel (601-634-4578), *Burton.Suedel@usace.army.mil*). This technical note should be cited as follows:

> Wilkens, J. L., B. C. Suedel. A. V. Davis and J. M. Corbino. 2018. *Improving Spatial Monitoring of Dredging Operations: A Small Unmanned Aerial System Application to Map Turbidity.* DOER Technical Notes Collection. ERDC/TN DOER-R27. Vicksburg, MS: U.S. Army Engineer Research and Development Center. *http://el.erdc.usace.army.mil/*.

REFERENCES

Clarke, D. G., and D. H. Wilber. 2008. Compliance monitoring of dredging-induced turbidity: defective designs and potential solutions. *Proceedings of the Western Dredging Association 28th Technical Conference*, WEDA, St. Louis, USA, 14 pp.

Congedo, L. 2016. Semi-automatic classification plugin documentation. Release 5.0.2.1, 201 pp. https://fromgistors.blogspot.com/p/semi-automatic-classification-plugin.html (Retrieved 3 January 2017).

Küng, O., C. Strecha, A. Beyeler, J-C. Zufferey, D. Floreano, P. Fua, and F. Gervaix. 2011. The accuracy of automatic photogrammetric techniques on ultra-light UAV imagery. In *UAV-g 2011-Unmanned Aerial Vehicle in Geomatics*, no. EPFL-CONF-168806. 2011.

Kutser, T., L. Metsamaa, E. Vahtmae, and R. Aps. 2007. Operative monitoring of the extent of dredging plumes in coastal ecosystems using MODIS satellite imagery. *Journal of Coastal Research*, SI 50 (Proceedings of the 9th International Coastal Symposium), 180–184. Gold Coast, Australia, ISSN 0749.0208.

Legleiter, C. J., M. Tedesco, L. C. Smith, A. E. Behar, and B. T. Overstreet. 2014. Mapping the bathymetry of supraglacial lakes and streams on the Greenland ice sheet using field measurements and high-resolution satellite images. *The Cryosphere* 8:215–228. DOI: 10.5164/tc-8-215-2014.

Lui, Y., Md. A. Islam, and J. Gao. 2003. Quantification of shallow water quality parameters by means of remote sensing. Progress in Physical Geography 27(1):24–43. DOI: 10.1191/0309133303pp357ra.

Lowe, D. G. 2004. Distinctive image features from scale-invariant keypoints. *International Journal of Computer Vision* 60(2):91–110.

Pruitt, B. A. 2003. Uses of turbidity by States and Tribes. In *Proceedings of the Federal Interagency Workshop on Turbidity and Other Sediment Surrogates*, USGS, April 30-May 2, 2002, Reno, NV. 31–46. http://water.usgs.gov/pubs/circ/2003/circ1250/.

Puckette, T. P. 1998. *Evaluation of dredged material plumes physical monitoring techniques*. DOER Technical Note Collection. ERDC TN-DOER-E5. Vicksburg MS: U.S. Army Engineer Research and Development Center. http://el.erdc.usace.army.mil/.

Reine, K. J., D. D. Dickerson, and D. G. Clarke. 1998. *Environmental windows associated with dredging operations*. DOER Technical Notes Collection. ERDC TN DOER-E2. Vicksburg, MS: U.S. Army Engineer Research and Development Center. http://el.erdc.usace.army.mil/.

Roberts, A., C. Kirman, and L. Lesack. 1995. Suspended sediment concentration estimation from multi-spectral video imagery, *International Journal of Remote Sensing* 16(13) 2439–2455. DOI: 10.1080/01431169508954568.

Roze, A., J. C. Zufferey, A. Beyeler, and A. McClellan. 2014. eBee RTK accuracy assessment (white paper). https://www.sensefly.com/fileadmin/user_upload/sensefly/documents/eBee-RTK-Accuracy-Assessment.pdf. (Retrieved on 3 January 2017)

Suedel, B. C., J. Kim, D. G. Clarke and I. Linkov. 2008. A risk-informed decision framework for setting environmental windows for dredging projects. *Science of the Total Environment* 403(1-3):1–11. https://doi.org/10.1016/j.scitotenv.2008.04.055

Tedesco, M., and N. Steiner. 2011. In-situ multispectral and bathymetric measurements over a supraglacial lake in western Greenland using a remotely controlled watercraft. *The Cryosphere* 5(2):445–452. DOI:10.5194/tc-5-445-2011.

Watts, A. C., J. H. Perry, S. E. Smith, M. A. Burgess, B. E. Wilkinson, Z. Szantoi, P. G. Ifju, and H. F. Percival. 2010. Small unmanned aircraft systems for low-altitude aerial surveys. *Journal of Wildlife Management* 74(7):1614–1619. https://doi.org/10.2193/2009-425

Vogt, M. C., M. E. Vogt. 2016. Near-remote sensing of water turbidity using small unmanned aircraft systems. *Environmental Practice* 18(1):18–31. https://doi.org/10.1017/S1466046615000459.

NOTE: *The contents of this technical note are not to be used for advertising, publication, or promotional purposes. Citation of trade names does not constitute an official endorsement or approval of the use of such products.*